TOMOGRAPHY® RESEARCH ARTICLE

Use of Indicator Dilution Principle to Evaluate Accuracy of Arterial Input Function Measured With Low-Dose Ultrafast Prostate Dynamic Contrast-Enhanced MRI

Shiyang Wang[1], Xiaobing Fan[1], Yue Zhang[1], Milica Medved[1], Dianning He[1,2], Ambereen Yousuf[1], Ernest Jamison[1], Aytekin Oto[1], and Gregory S. Karczmar[1]

[1]Department of Radiology, University of Chicago, Chicago, IL and [2]Sino-Dutch Biomedical and Information Engineering School, Northeastern University, Shenyang, China

Corresponding Author:
Gregory S. Karczmar, PhD
Department of Radiology, University of Chicago, 5841 S. Maryland Avenue, MC2026, Chicago, IL, USA 60637;
E-mail: gskarczm@uchicago.edu

Key Words: arterial input function, low dose DCE-MRI, cardiac output, indicator dilution principle

Abbreviations: Arterial input function (AIF), dynamic contrast-enhanced (DCE), magnetic resonance imaging (MRI), cardiac output (CO), cardiac MRI (CMRI), cardiac output from CMRI (CO_{CMRI}), cardiac output from DCE-MRI (CO_{DCE}), computed tomography (CT), repetition time (TR), echo time (TE), flip angle (FA), field of view (FOV), gadolinium (Gd), region of interest (ROI), standard deviation (SD)

ABSTRACT

Accurately measuring arterial input function (AIF) is essential for quantitative analysis of dynamic contrast-enhanced (DCE) magnetic resonance imaging (MRI). We used the indicator dilution principle to evaluate the accuracy of AIF measured directly from an artery following a low-dose contrast media ultrafast DCE-MRI. In total, 15 patients with biopsy-confirmed localized prostate cancers were recruited. Cardiac MRI (CMRI) and ultrafast DCE-MRI were acquired on a Philips 3 T Ingenia scanner. The AIF was measured at iliac arties following injection of a low-dose (0.015 mmol/kg) gadolinium (Gd) contrast media. The cardiac output (CO) from CMRI (CO_{CMRI}) was calculated from the difference in ventricular volume at diastole and systole measured on the short axis of heart. The CO from DCE-MRI (CO_{DCE}) was also calculated from the AIF and dose of the contrast media used. A correlation test and Bland–Altman plot were used to compare CO_{CMRI} and CO_{DCE}. The average (±standard deviation [SD]) area under the curve measured directly from local AIF was 0.219 ± 0.07 mM·min. The average (±SD) CO_{CMRI} and CO_{DCE} were 6.52 ± 1.47 L/min and 6.88 ± 1.64 L/min, respectively. There was a strong positive correlation ($r = 0.82$, $P < .01$) and good agreement between CO_{CMRI} and CO_{DCE}. The CO_{DCE} is consistent with the reference standard CO_{CMRI}. This indicates that the AIF can be measured accurately from an artery with ultrafast DCE-MRI following injection of a low-dose contrast media.

INTRODUCTION

Dynamic contrast-enhanced (DCE) magnetic resonance imaging (MRI) has been widely used for cancer diagnosis, as well as to quantitatively and noninvasively estimate a lesion's physiological characteristics (1-5). Quantitative DCE-MRI analysis is usually performed by using a pharmacokinetic model to obtain transfer rate constants, such as K^{trans} (forward volume transfer constant) and k_{ep} (reverse reflux rate constant between extracellular space and plasma) to characterize cancers (6, 7). However, variations of arterial input function (AIF) have a strong impact on calculations of physiological parameters (8-11). To extract reliable physiological parameters, an accurate AIF must be measured for each patient to account for variations in cardiac output (CO), systemic vascular function, and injection protocol (8). Unfortunately, there is potential for significant error in AIF measurements owing to partial volume effects, respiratory motions, inflow artifacts, dose-dependent T2*, and water exchange effects (12-14). To avoid problems with accurate measurement of patient-specific AIFs, a population AIF is often used in quantitative DCE-MRI data analysis (15-17). However, this does not account for the large interpatient and interscan variability, and this makes it difficult to compare physiological parameters between patients or measure changes in each patient over time (18, 19).

Several investigators have developed methods for quantitatively measuring patient-specific AIFs with MRI (10, 20, 21). However, the accuracy of the measured AIF was not verified in most studies. Previous studies reported that using CO combined with capillary input function improved the estimation of pharmacokinetic parameters for liver (22). By applying the indicator dilution principle (23) to constrain the area under the first pass of the AIF, Zhang et al. (24) reported a 3-fold higher precision in

ISSN 2379-1381 https://doi.org/10.18383/j.tom.2019.00004

calculating tumor perfusion parameters (K^{trans} and v_e). Di Giovanni et al. (25) reported a method for estimating perfusion parameters in patients with breast cancer using a T2*-weighted DCE data set optimized with CO. All of these studies applied the indicator dilution principle to optimize (scale) AIF based on each patient's CO. The need for this adjustment indicates that there were significant errors in the directly measured AIFs. Several studies also compared the AIFs measured from DCE-MRI and DCE computed tomography (CT) scans (26-28), where the AIF obtained from CT was treated as gold standard. However, the accuracy of this comparison was limited because of radiation dose constraints on temporal sampling with dynamic CT. In addition, this approach to validation entails radiation and additional contrast media.

In the present study, the indicator dilution principle was used to verify the accuracy of the AIF directly measured at the iliac arties following injection of a very low-dose contrast media. The key difference from previous studies is to verify, but not to optimize (scale), the measured AIF. The CO of each patient was directly calculated from short-axis cardiac MRI (CMRI) data. A high temporal resolution (ultrafast) prostate DCE-MRI scan was acquired with a low-dose contrast media, that is, 15% of the conventional amount, to avoid errors due to T2* changes and water exchange.

METHODOLOGY

Patient

This study was approved by the Institutional Review Board. Patients were enrolled from January 01, 2017, to March 01, 2018. Informed consent was obtained from all patients before conducting any study procedures. All patients enrolled in this study had prostate cancer proven by TRUS (transrectal ultrasound)-guided biopsy and were scheduled for radical prostatectomy at our hospital. Patients with previous treatments (radiation or chemotherapy) for prostate cancer, any type of bioimplant, moderate or high anxiety and/or claustrophobia, and contraindications for MRI or CT including impaired renal function (GFR $<$ 60 mL/min) were excluded from the study.

Fifteen patients (average age, 59 years; range, 47–73 years; average weight, 96.7 kg; range, 79–132 kg) received both cardiac MRI (CMRI) and a subsequent prostate DCE-MRI scans on the same day. The cohort comprised Gleason grade 6–9 lesions including: Gleason score (GS) 3 + 3 (n = 2), GS 3 + 4 (n = 11), GS 4 + 3 (n = 6), and GS 4 + 5 (n = 1).

CMRI and Prostate DCE-MRI Scan Protocols

Both CMRI and low-dose (0.015 mmol/kg of gadobenate dimeglumine) ultrafast DCE-MRI were acquired on the same Philips 3 T Ingenia scanner (Philips Healthcare, Best, Netherlands). A gradient echo sequence (B-TFE) was used for imaging the cardiac short axis (repetition time [TR] = 3.2 milliseconds, echo time [TE] = 1.6 milliseconds, flip angle [FA] = 45°, field of view [FOV] = 30 × 30 cm^2, slices = 14, phases = 30–40, gap = 0, in-plane resolution = 1.0 × 1.0 × 8 mm^3, maximum dynamic time = 800–1025 milliseconds).

Prostate MRI scans were performed approximately 30 minutes after the CMRI scan. First, clinically required prostate MRI scans, including high-resolution axial T2-weighted MRI and diffusion-weighted imaging, were acquired. Then variable FA 3D-FFE-T1 scans (TE/TR = 2.3/12 milliseconds; FA = 3°, 5°, 10°, 15°, 20°, 30°; FOV = 25 × 39 cm^2; in-plane resolution = 1.25 × 1.75 mm^2; thickness = 3.5 mm) were acquired for the calculation of native T1. Next, 150 axial ultrafast DCE-MRI using an mDixon sequence (27, 29, 30) (TE1/TE2/TR = 1.5/2.8/4.2 milliseconds, FA = 10°, FOV = 18 × 37 × 8 cm^3, in-plane resolution = 1.5 × 2.8 × 3.5 mm^3, temporal resolution = 1.5 s) were acquired over 225 seconds. A small dose (15% of the conventional dose, 0.015 mmol/kg) of Gd-based contrast media (gadobenate dimeglumine) was injected into the patients' left arm median cubital vein with a power injector at an injection duration of ~1.5 seconds, and followed by a 20-mL saline flush. The first 10 sets of ultrafast DCE-MRI images were precontrast scans used as baseline images. An approximate standard dose of contrast media was injected ~5 minutes after the low-dose contrast media DCE-MRI. Data from the standard dose were not used in the work reported here.

CO Measurements from CMRI

Electrodes were attached on the patient's chest during the CMRI scan to monitor the patient's electrocardiogram. The CO from CMRI (CO_{CMRI}) was calculated on the basis of the difference between ventricular volume at diastole and at systole measured on the short axis of the heart using the following formula (31-33):

$$CO_{CMRI} = HR \times (V_{ED} - V_{ES}) \quad (1)$$

where V_{ED} (L) is the volume at the end of diastole, V_{ES} (L) is the volume at the end of systole, and HR (beats/min, bpm) is the patient's heart rate recorded from electrocardiogram.

Contrast Media Concentration Measurements from DCE-MRI

For all DCE-MRI slices, the contrast media concentration as a function of time was calculated by using a previously published method (34) based on MRI TR, FA, native T1, and baseline signal. The native T1 was calculated by using the acquired precontrast dual-TR and variable flip angle images as previously described (35-37). The relaxivity of the contrast media of 5.5 L/mmol/s (38) was used to calculate the Gd concentration in millimolar units. AIFs were extracted from ultrafast DCE-MRI by manually tracing the region of interest (ROI) over the left and right iliac arteries. The shapes of the ROIs changed on different slices owing to blood vessel visibility variations on DCE-MRI. The average (±standard deviation [SD]) size of the ROI was 18 ± 6 pixels. The vessel walls could be easily excluded from the contour because they had different contrasts compared with the vessel lumen. The average contrast media concentration from the left and right iliac arteries was calculated and used as the AIF for the patient.

The accuracy of the measured AIF was verified by using the indicator dilution theory, which states that the area under a curve of the blood plasma contrast media concentration during the first-pass perfusion is constant in every vessel (25). The CO measured from CMRI versus DCE-MRI should be the same if the AIF is accurately measured.

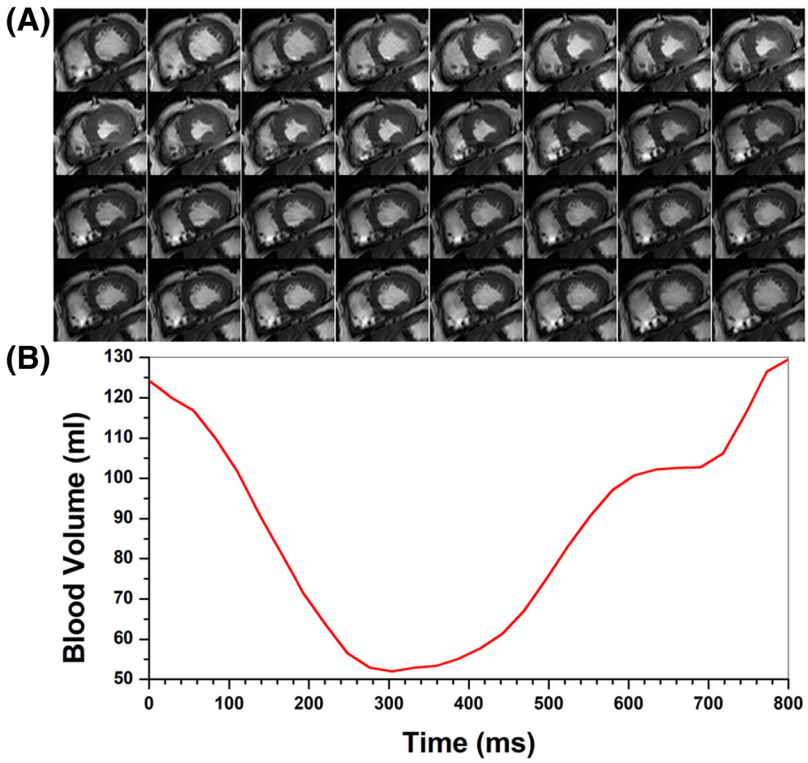

Figure 1. Cardiac output (CO) calculation from cardiac magnetic resonance imaging (CMRI) where (A) is a a section of short-axis CMRI during a full CO. Row 2, column 2, image shows the minimum cross-section area during the end of the systolic period; row 4, column 8, image shows the maximum cross-section area during the end of the diastolic period; (B) is the plot of ventricular volume measured from short-axis CMRI.

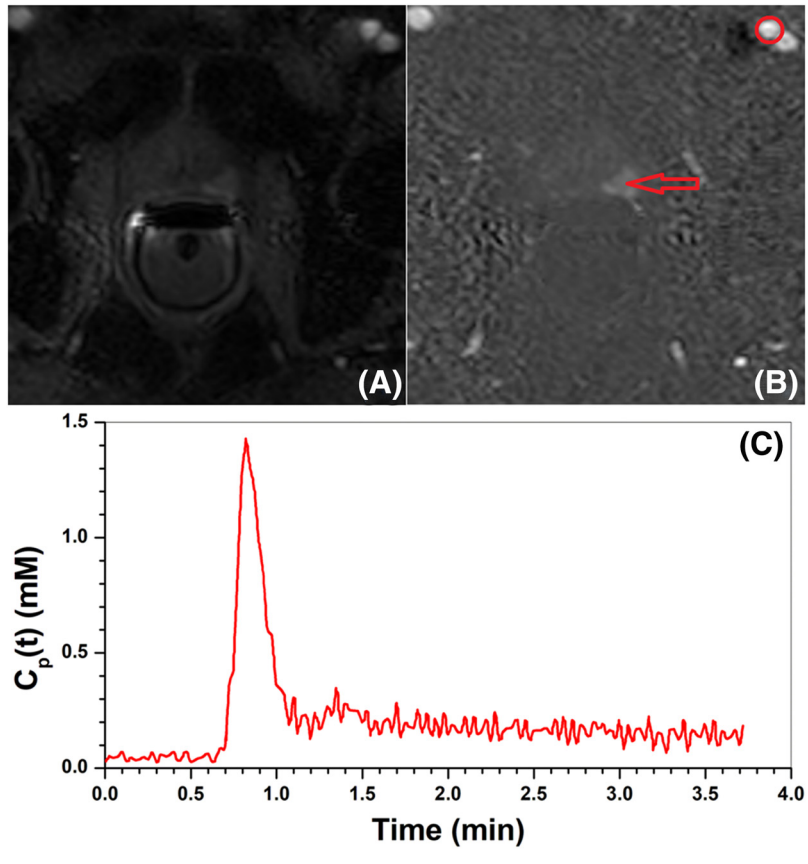

Figure 2. The ultrafast dynamic contrast-enhanced (DCE) image following a low dose of contrast media from the same patient (at the 40th dynamic scan) (A), the subtracted dynamic image from baseline shows early enhancement in prostatic carcinoma (red arrow) (B), and the AIF generated from iliac artery (red circle) from the ultrafast DCE-MRI data (C).

Table 1. Patients' Heart Rate, Area Under the Curve Measured Directly from Local AIF, and CO_{DCE} and CO_{CMRI}

No.	Heart Rate (beats/min)	AIF (AUC) (mM·min)	CO_{DCE} (L/min)	CO_{CMRI} (L/min)
1	66	0.228	5.92	5.90
2	68	0.252	5.63	5.90
3	73	0.203	6.37	5.70
4	53	0.189	6.88	7.70
5	47	0.440	2.73	3.99
6	82	0.175	7.20	6.54
7	60	0.174	7.47	5.80
8	63	0.170	8.24	7.74
9	67	0.225	6.67	6.01
10	60	0.229	6.81	5.50
11	65	0.163	8.56	7.90
12	61	0.149	8.66	7.92
13	65	0.266	5.64	5.10
14	58	0.169	9.67	9.96
15	51	0.247	6.80	6.10

CO Measurements from Ultrafast DCE-MRI

The CO from ultrafast DCE-MRI (CO_{DCE}) was calculated from the AIF and the dose of contrast media (24):

$$CO_{DCE} = Q \Big/ \int C_p(t)dt \qquad (2)$$

where Q (mmol) is the amount of the contrast media injected, and $C_P(t)$ (mM) is the contrast media concentration in the blood plasma. The area under the "first pass" of contrast media circulation was used for integration, that is, from baseline immediately before bolus arrival to the end of the first pass of the contrast media bolus.

Data Analysis

Paired Student *t*-test was used to compare the CO_{CMRI} and ultrafast CO_{DCE}. Pearson correlation test was performed to examine whether there is a linear relationship between CO_{CMRI} and CO_{DCE}. The agreements between CO_{CMRI} and CO_{DCE} values were evaluated using Bland–Altman analysis. $P < .05$ was considered significant.

RESULTS

CMRI was acquired first for calculating CO as a reference standard. Figure 1A shows typical images of the short axis of the heart during a cardiac cycle. The image in row 2, column 2, has the minimum cross-sectional area during the end of the systolic period; the image in row 4, column 8, has the maximum cross-sectional area during the end of the diastolic period. The corresponding plot of ventricular volumes measured from short axis of the heart as a function of time is shown in Figure 1B. The V_{ED} and V_{ES} used in equation (1) for calculating CO_{CMRI} were the maximum and minimum values, respectively, in the plot.

After CMRI, prostate DCE-MRI was acquired, and the AIF was measured directly from the iliac arteries. Figure 2A shows the ultrafast DCE image (at the 40th dynamic scan) from the same patient as shown in Figure 1. The subtracted dynamic image (Figure 2B) from the baseline (averaged from all baseline frames) shows early enhancement in prostatic carcinoma (red arrow), and the AIF traced from the iliac artery (red circle) is shown in Figure 2C. The first and second pass peaks of the contrast bolus can be clearly seen in the AIF despite limited signal-to-noise ratio owing to injection of the low-dose contrast media.

This data analysis procedure was applied to data from all 15 patients. Table 1 lists the patients' heart rate, the area under the curve measured directly from local AIF, and the calculated CO_{DCE} and CO_{CMRI} as the reference standard. The average (±SD) area under the curve measured directly from local AIF obtained from ultrafast DCE-MRI is 0.219 ± 0.07 mM·min. The average (±SD) COs calculated from CMRI and DCE-MRI are 6.52 ± 1.47 L/min and 6.88 ± 1.64 L/min, respectively. Both CO_{CMRI} and CO_{DCE} vary by over a factor of 2 in this group of patients. Figure 3A shows the scatter plot of the CO_{CMRI} vs CO_{DCE}. There are strong positive correlations ($r = 0.82$, $P < .01$) between the CO_{CMRI} and CO_{DCE}. The corresponding Bland–Altman plot shows good agreement between the two CO measurements (Figure 3B) with bias of 0.37 (L/min) and limits of agreement between −1.14 to 1.87 (L/min).

DISCUSSION

The indicator dilution principle was used to verify the accuracy of AIF measured at iliac arties from ultrafast DCE-MRI scan after injection of the low-dose contrast media. The subject's CO was directly measured from CMRI before the prostate DCE-MRI scan. We showed that the CO measured from ultrafast DCE-MRI is consistent with the "gold standard" CO measured from the short-axis CMRI. Our results show that AIF can be accurately measured directly from an artery with ultrafast DCE-MRI following injection of a low-dose contrast media. Accurate measurement of AIF for individual patients is critical for pharmacokinetic analysis.

The present results also suggest some clinical and diagnostic advantages for use of a low-dose contrast media DCE-MRI (39). The association between Gd-based contrast media administration and nephrogenic systemic fibrosis has been a concern for patients with renal failure. In a retrospective study, acute renal failure was reported after high-dose (≥0.2 mmol/kg) Gd injection for patients with an eGFR lower than 30 mL/min (40). It has also been reported that high-dose Gd injection contributed to an increased risk of nephrogenic systemic fibrosis (41). There are increasing concerns regarding intracellular accumulation of Gd-based contrast media (42). Therefore, a low-dose contrast media is preferred to minimize the risk (39). In addition, a standard dose of contrast media may lead to erroneous estimation of AIF owing to the high concentration of the contrast, water exchange effects, and T2* effects (12-14). The AIF measured from a low-dose contrast media may reduce such errors, as demonstrated by the present study results. In addition, this was previously shown by comparing results from ultrafast DCE-MRI with those from DCE-CT with 120-mL Iohexol in 20 patients with prostate cancer (27). Previous work from this group showed

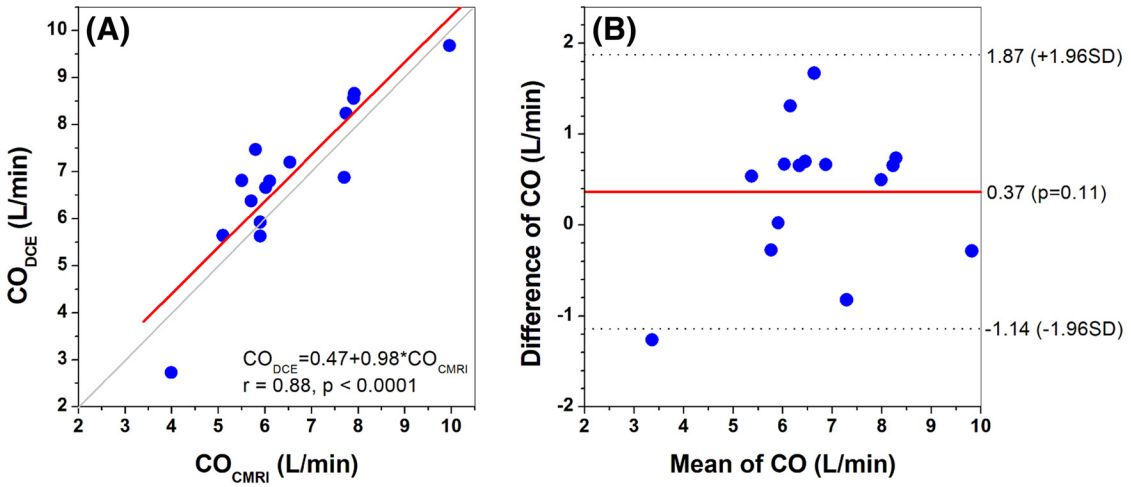

Figure 3. The scatter plot (A) shows the correlation (red line) of CO measured from the CMRI and ultrafast DCE-MRI. The corresponding Bland–Altman plot is shown in (B). The solid red line represents the mean difference ($CO_{DCE} - CO_{CMRI}$), and the dashed lines represent the lower and upper limits of agreement, defined by a range of $\pm 1.96 \times$ SD (95% confidence interval) around the mean. The *P*-value appearing beside the mean line on the plot indicates the probability of bias that differs from zero.

that low-dose Gd contrast distinguishes prostate cancer from benign prostate tissue more effectively than a standard dose on the basis of the signal enhancement rate; this diagnostic accuracy is similar on qualitative assessments (39).

CO is an important physiological parameter that directly relates to the metabolism of the entire organism (43). Results from the current group of patients show that there is a wide variation in CO (over a factor of 2) and this will result in large errors in pharmacokinetic parameters if it is not properly accounted for. A separate magnetic resonance sequence is often used to obtain CO. Our method with a low-dose contrast media and ultrafast DCE of the abdomen can provide accurate AIF *and* measure CO simultaneously, without performing additional scans, and with minimal exposure to contrast media.

Our measurements of CO and AIF are not perfect. For example, the native T1 measurement has a strong effect on Gd concentration calculation and AIF curve shape. This is because other parameters used in the calculation of contrast media concentration are dependent on MRI acquisition parameters. In addition, the native T1 must be determined from additional MRI scans that can contribute error. The CMRI slice thickness (8 mm) can be reduced to more accurately measure the diastolic and systolic volume for more accurate CO calculation. The measurement errors in V_{ED} and V_{ES} would only linearly affect CO_{CMRI} calculations, which were naturally smaller than errors in CO_{DCE} calculations owing to the many calculations involved.

In conclusion, accurately measuring of the AIF is essential for quantitative DCE-MRI. Here we compared the CO measured from CMRI as reference standard with the CO determined from measurement of the AIF with ultrafast DCE-MRI. The results validated the accuracy of the AIF measured at iliac arties following injection of a low-dose (0.015 mmol/kg) Gd contrast media. The low dose chosen for this study may not be optimal for measuring AIF and/or for the diagnosis of cancers. More studies are needed to determine the optimal low dose for both accurately measuring the AIF and estimating physiological parameters.

ACKNOWLEDGMENTS

This research is supported by the National Institutes of Health (Grant numbers: R01CA218700, U01CA142565, R01CA172801, and S10OD018448) and the University of Chicago Comprehensive Cancer Center from the National Cancer Institute Cancer Center Support Grant P30CA014599.

Disclosures: No disclosures to report.

Conflict of Interest: The authors have no conflict of interest to declare.

REFERENCES

1. Abramson RG1, Li X, Hoyt TL, Su PF, Arlinghaus LR, Wilson KJ, Abramson VG, Chakravarthy AB, Yankeelov TE. Early assessment of breast cancer response to neoadjuvant chemotherapy by semi-quantitative analysis of high-temporal resolution DCE-MRI: preliminary results. Magn Reson Imaging. 2013;31:1457–1464.
2. Alonzi R, Padhani AR, Allen C. Dynamic contrast enhanced MRI in prostate cancer. Eur J Radiol. 2007;63:335–350.
3. Gollub MJ, Gultekin DH, Akin O, Do RK, Fuqua JL 3rd, Gonen M, Kuk D, Weiser M, Saltz L, Schrag D, Goodman K, Paty P, Guillem J, Nash GM, Temple L, Shia J, Schwartz LH. Dynamic contrast enhanced-MRI for the detection of pathological complete response to neoadjuvant chemotherapy for locally advanced rectal cancer. Eur Radiol. 2012;22:821–831.
4. Pinker K, Bogner W, Baltzer P, Trattnig S, Gruber S, Abeyakoon O, Bernathova M, Zaric O, Dubsky P, Bago-Horvath Z, Weber M, Leithner D, Helbich TH. Clinical application of bilateral high temporal and spatial resolution dynamic contrast-enhanced magnetic resonance imaging of the breast at 7 T. Eur Radiol. 2014; 24:913–920.
5. Vos EK, Litjens GJ, Kobus T, Hambrock T, Hulsbergen-van de Kaa CA, Barentsz JO, Huisman HJ, Scheenen TW. Assessment of prostate cancer aggressiveness

using dynamic contrast-enhanced magnetic resonance imaging at 3 T. Eur Urol. 2013;64:448–455.
6. Patankar TF, Haroon HA, Mills SJ, Baleriaux D, Buckley DL, Parker GJ, Jackson A. Is volume transfer coefficient (K(trans)) related to histologic grade in human gliomas? AJNR Am J Neuroradiol. 2005;26:2455–2465.
7. Tofts PS, Brix G, Buckley DL, Evelhoch JL, Henderson E, Knopp MV, Larsson HB, Lee TY, Mayr NA, Parker GJ, Port RE, Taylor J, Weisskoff RM. Estimating kinetic parameters from dynamic contrast-enhanced T(1)-weighted MRI of a diffusable tracer: standardized quantities and symbols. J Magn Reson Imaging. 1999;10:223–232.
8. Fedorov A, Fluckiger J, Ayers GD, Li X, Gupta SN, Tempany C, Mulkern R, Yankeelov TE, Fennessy FM. A comparison of two methods for estimating DCE-MRI parameters via individual and cohort based AIFs in prostate cancer: a step towards practical implementation. Magn Reson Imaging. 2014;32:321–329.
9. Huang W, Chen Y, Fedorov A, Li X, Jajamovich GH, Malyarenko DI, Aryal MP, LaViolette PS, Oborski MJ, O'Sullivan F, Abramson RG, Jafari-Khouzani K, Afzal A, Tudorica A, Moloney B, Gupta SN, Besa C, Kalpathy-Cramer J, Mountz JM, Laymon CM, Muzi M, Schmainda K, Cao Y, Chenevert TL, Taouli B, Yankeelov TE, Fennessy F, Li X. The impact of arterial input function determination variations on prostate dynamic contrast-enhanced magnetic resonance imaging pharmacokinetic modeling: a multicenter data analysis challenge. Tomography. 2016;2:56–66.
10. Sanz-Requena R, Prats-Montalbán JM, Marti-Bonmati L, Alberich-Bayarri A, Garcia-Marti G, Perez R, Ferrer A. Automatic individual arterial input functions calculated from PCA outperform manual and population-averaged approaches for the pharmacokinetic modeling of DCE-MR images. J Magn Reson Imaging. 2015;42:477–487.
11. Wang S, Fan X, Medved M, Pineda FD, Yousuf A, Oto A, Karczmar GS. Arterial input functions (AIFs) measured directly from arteries with low and standard doses of contrast agent, and AIFs derived from reference tissues. Magn Reson Imaging. 2016;34:197–203.
12. Hansen AE, Pedersen H, Rostrup E, Larsson HB. Partial volume effect (PVE) on the arterial input function (AIF) in T1-weighted perfusion imaging and limitations of the multiplicative rescaling approach. Magn Reson Med. 2009;62:1055–1059.
13. Kleppesto M, Larsson C, Groote I, Salo R, Vardal J, Courivaud F, Bjørnerud A. T2*-correction in dynamic contrast-enhanced MRI from double-echo acquisitions. J Magn Reson Imaging. 2014;39:1314–1319.
14. Roberts C, Little R, Watson Y, Zhao S, Buckley DL, Parker GJ. The effect of blood inflow and B(1)-field inhomogeneity on measurement of the arterial input function in axial 3D spoiled gradient echo dynamic contrast-enhanced MRI. Magn Reson Med. 2011;65:108–119.
15. McGrath DM, Bradley DP, Tessier JL, Lacey T, Taylor CJ, Parker GJ. Comparison of model-based arterial input functions for dynamic contrast-enhanced MRI in tumor bearing rats. Magn Reson Med. 2009;61:1173–1184.
16. Meng R, Chang SD, Jones EC, Goldenberg SL, Kozlowski P. Comparison between population average and experimentally measured arterial input function in predicting biopsy results in prostate cancer. Acad Radiol. 2010;17:520–525.
17. Parker GJ, Roberts C, Macdonald A, Buonaccorsi GA, Cheung S, Buckley DL, Jackson A, Watson Y, Davies K, Jayson GC. Experimentally-derived functional form for a population-averaged high-temporal-resolution arterial input function for dynamic contrast-enhanced MRI. Magn Reson Med. 2006;56:993–1000.
18. Beuzit L, Eliat PA, Brun V, Ferre JC, Gandon Y, Bannier E, Saint-Jalmes H. Dynamic contrast-enhanced MRI: Study of inter-software accuracy and reproducibility using simulated and clinical data. J Magn Reson Imaging. 2016;43:1288–1300.
19. Huang W, Li X, Chen Y, Li X, Chang MC, Oborski MJ, Malyarenko DI, Muzi M, Jajamovich GH, Fedorov A, Tudorica A, Gupta SN, Laymon CM, Marro KI, Dyvorne HA, Miller JV, Barbodiak DP, Chenevert TL, Yankeelov TE, Mountz JM, Kinahan PE, Kikinis R, Taouli B, Fennessy F, Kalpathy-Cramer J. Variations of dynamic contrast-enhanced magnetic resonance imaging in evaluation of breast cancer therapy response: a multicenter data analysis challenge. Transl Oncol. 2014;7:153–166.
20. Cron GO, Foottit C, Yankeelov TE, Avruch LI, Schweitzer ME, Cameron I. Arterial input functions determined from MR signal magnitude and phase for quantitative dynamic contrast-enhanced MRI in the human pelvis. Magn Reson Med. 2011;66:498–504.
21. Fennessy FM, Fedorov A, Penzkofer T, Kim KW, Hirsch MS, Vangel MG, Masry P, Flood TA, Chang MC, Tempany CM, Mulkern RV, Gupta SN. Quantitative pharmacokinetic analysis of prostate cancer DCE-MRI at 3T: comparison of two arterial input functions on cancer detection with digitized whole mount histopathological validation. Magn Reson Imaging. 2015;33:886–894.
22. Chouhan MD, Bainbridge A, Atkinson D, Punwani S, Mookerjee RP, Lythgoe MF, Taylor SA. Improved hepatic arterial fraction estimation using cardiac output correction of arterial input functions for liver DCE MRI. Phys Med Biol. 2017;62:1533–1546.
23. Zierler K. Indicator dilution methods for measuring blood flow, volume, and other properties of biological systems: a brief history and memoir. Ann Biomed Eng. 2000;28:836–848.
24. Zhang JL, Rusinek H, Bokacheva L, Chen Q, Storey P, Lee VS. Use of cardiac output to improve measurement of input function in quantitative dynamic contrast-enhanced MRI. J Magn Reson Imaging. 2009;30:656–665.
25. Di Giovanni P, Ahearn TS, Semple SI, Azlan CA, Lloyd WK, Gilbert FJ, Redpath TW. Use of a capillary input function with cardiac output for the estimation of lesion pharmacokinetic parameters: preliminary results on a breast cancer patient. Phys Med Biol. 201121;56:1743–1753.
26. Rata M, Collins DJ, Darcy J, Messiou C, Tunariu N, Desouza N, Young H, Leach MO, Orton MR. Assessment of repeatability and treatment response in early phase clinical trials using DCE-MRI: comparison of parametric analysis using MR- and CT-derived arterial input functions. Eur Radiol. 2016;26:1991–1998.
27. Wang S, Lu Z, Fan X, Medved M, Jiang X, Sammet S, Yousuf A, Pineda F, Oto A, Karczmar GS. Comparison of arterial input functions measured from ultra-fast dynamic contrast enhanced MRI and dynamic contrast enhanced computed tomography in prostate cancer patients. Phys Med Biol. 2018;63:03NT1.
28. Yang C, Stadler WM, Karczmar GS, Milosevic M, Yeung I, Haider MA. Comparison of quantitative parameters in cervix cancer measured by dynamic contrast-enhanced MRI and CT. Magn Reson Med. 2010;63:1601–1609.
29. Dixon WT. Simple proton spectroscopic imaging. Radiology. 1984;153:189–194.
30. Le Y, Dale B, Akisik F, Koons K, Lin C. Improved T1, contrast concentration, and pharmacokinetic parameter quantification in the presence of fat with two-point Dixon for dynamic contrast-enhanced magnetic resonance imaging. Magn Reson Med. 2016;75:1677–1684.
31. Hundley WG, Li HF, Hillis LD, Meshack BM, Lange RA, Willard JE, Landau C, Peshock RM. Quantitation of cardiac output with velocity-encoded, phase-difference magnetic resonance imaging. Am J Cardiol. 1995;75:1250–1255.
32. Lin HY, Freed D, Lee TW, Arora RC, Ali A, Almoustadi W, Xiang B, Wang F, Large S, King SB, Tomanek B, Tian G. Quantitative assessment of cardiac output and left ventricular function by noninvasive phase-contrast and cine MRI: validation study with invasive pressure-volume loop analysis in a swine model. J Magn Reson Imaging. 2011;34:203–210.
33. Vincent JL. Understanding cardiac output. Crit Care. 2008;12:174.
34. Dale BM, Jesberger JA, Lewin JS, Hillenbrand CM, Duerk JL. Determining and optimizing the precision of quantitative measurements of perfusion from dynamic contrast enhanced MRI. J Magn Reson Imaging. 2003;18:575–584.
35. Fram EK, Herfkens RJ, Johnson GA, Glover GH, Karis JP, Shimakawa A, Perkins TG, Pelc NJ. Rapid calculation of T1 using variable flip angle gradient refocused imaging. Magn Reson Imaging. 1987;5:201–208.
36. Manuel A, Li W, Jellus V, Hughes T, Prasad PV. Variable flip angle-based fast three-dimensional T1 mapping for delayed gadolinium-enhanced MRI of cartilage of the knee: need for B1 correction. Magn Reson Med. 2011;65:1377–1383.
37. Pineda FD, Medved M, Fan X, Karczmar GS. B1 and T1 mapping of the breast with a reference tissue method. Magn Reson Med. 2016;75:1565–1573.
38. Rohrer M, Bauer H, Mintorovitch J, Requardt M, Weinmann H-J. Comparison of magnetic properties of MRI contrast media solutions at different magnetic field strengths. Invest Radiol. 2005;40:715–724.
39. He D, Chatterjee A, Fan X, Wang S, Eggener S, Yousuf A, Antic T, Oto A, Karczmar GS. Feasibility of dynamic contrast-enhanced magnetic resonance imaging using low-dose gadolinium: comparative performance with standard dose in prostate cancer diagnosis. Invest Radiol. 2018;53:609–615.
40. Prince MR, Zhang H, Morris M, MacGregor JL, Grossman ME, Silberzweig J, DeLapaz RL, Lee HJ, Magro CM, Valeri AM. Incidence of nephrogenic systemic fibrosis at two large medical centers. Radiology. 2008;248:807–816.
41. Broome DR, Girguis MS, Baron PW, Cottrell AC, Kjellin I, Kirk GA. Gadodiamide-associated nephrogenic systemic fibrosis: why radiologists should be concerned. AJR Am J Roentgenol. 2007;188:586–592.
42. Ramalho J, Semelka RC, Ramalho M, Nunes RH, AlObaidy M, Castillo M. Gadolinium-based contrast agent accumulation and toxicity: an update. AJNR Am J Neuroradiol. 2016;37:1192–1198.
43. Carlsson M, Andersson R, Bloch KM, Steding-Ehrenborg K, Mosen H, Stahlberg F, Stahlberg F, Ekmehag B, Arheden H. Cardiac output and cardiac index measured with cardiovascular magnetic resonance in healthy subjects, elite athletes and patients with congestive heart failure. J Cardiovasc Magn Reson. 2012;14:51.